Journal of Molecular and Cellular Cardiology 188 (2024) 65–78

Contents lists available at ScienceDirect

Journal of Molecular and Cellular Cardiology

journal homepage: www.elsevier.com/locate/yjmcc

NCoR1 limits angiogenic capacity by altering Notch signaling

Tom Teichmann [a,b], Pedro Malacarne [a,b], Simonida Zehr [a,b], Stefan Günther [c], Beatrice Pflüger-Müller [a,b], Timothy Warwick [a,b,*], Ralf P. Brandes [a,b,*]

[a] Institute for Cardiovascular Physiology, Goethe University, Frankfurt am Main 60590, Germany
[b] German Center for Cardiovascular Research (DZHK), Partner site Rhein Main, Frankfurt am Main, Germany
[c] Max-Planck-Institute for Heart- and Lung Research (MPI-HLR), Bad Nauheim 61231, Germany

ARTICLE INFO

Keywords:
NCoR1
Endothelial cells
Notch signaling
Angiogenesis

ABSTRACT

Corepressors negatively regulate gene expression by chromatin compaction. Targeted regulation of gene expression could provide a means to control endothelial cell phenotype. We hypothesize that by targeting corepressor proteins, endothelial angiogenic function can be improved. To study this, the expression and function of nuclear corepressors in human umbilical vein endothelial cells (HUVEC) and in murine organ culture was studied. RNA-seq revealed that nuclear receptor corepressor 1 (NCoR1), silencing mediator of retinoid and thyroid hormone receptors (SMRT) and repressor element-1 silencing transcription factor (REST) are the highest expressed corepressors in HUVECs. Knockout and knockdown strategies demonstrated that the depletion of NCoR1 increased the angiogenic capacity of endothelial cells, whereas depletion of SMRT or REST did not. Interestingly, the effect was VEGF signaling independent. NCoR1 depletion significantly upregulated angiogenesis-associated genes, especially tip cell genes, including *ESM1*, *DLL4* and *NOTCH4*, as observed by RNA- and ATAC-seq. Confrontation assays comparing cells with and without NCoR1-deficiency revealed that loss of NCoR1 promotes a tip-cell position during spheroid sprouting. Moreover, a proximity ligation assay identified NCoR1 as a direct binding partner of the Notch-signaling-related transcription factor RBPJk. Luciferase assays showed that siRNA-mediated knockdown of *NCOR1* promotes RBPJk activity. Furthermore, NCoR1 depletion prompts upregulation of several elements in the Notch signaling cascade. Downregulation of *NOTCH4*, but not *NOTCH1*, prevented the positive effect of *NCOR1* knockdown on spheroid outgrowth. Collectively, these data indicate that decreasing *NCOR1* expression is an attractive approach to promote angiogenic function.

1. Introduction

Eukaryotic gene expression is controlled on numerous layers. One of the best-characterized control mechanisms regards to the dynamics of chromatin state. Heterochromatin formation is the condensation of chromatin showing a reduced accessibility for the transcriptional machinery, suppressing gene expression, whereas euchromatin formation involves chromatin relaxation and facilitates gene expression [1]. The switch between these two states is facilitated by two classes of enzymes, the histone acetyltransferases (HATs) and the histone deacetylases (HDACs) [2]. These enzymes alter DNA accessibility through post-translational modifications (PTMs), namely acetylation [3]. Although histone modifiers can be directly recruited to the DNA, an interaction with chromatin modifying complexes such as corepressors or coactivators is common [4]. Such coregulators act as scaffolding platforms for an array of proteins, forming a chromatin remodeling complex, which is then recruited by transcription factors to sites of gene regulation, such as promoters and enhancers [5]. Binding of coregulators occurs genome-wide and specific targeting therefore should have a strong impact on the cellular phenotype. For example, it may induce a switch of the cellular phenotype from a quiescent into an activated state [6].

The 'nuclear receptor corepressor 1' (NCoR1) and its paralog 'silencing mediator of retinoic acid and thyroid hormone receptor' (SMRT, NCoR2) belong to the best characterized corepressors. While the global deletion of either of these corepressors is embryonically lethal in mice, tissue specific and conditional deletions are viable [7,8]. Using these approaches, NCoR1 has been shown to be essential for T-cell development by promoting thymocyte survival [9]. Skeletal muscle-specific loss of NCoR1 increases muscle mass and mitochondrial activity [10]. Knockout of NCoR1 in cardiomyocytes results in cardiac

* Corresponding authors at: Institut für Kardiovaskuläre Physiologie, Fachbereich Medizin der Goethe Universität, Theodor-Stern-Kai 7, Frankfurt am Main 60590, Germany
E-mail addresses: warwick@med.uni-frankfurt.de (T. Warwick), r.brandes@em.uni-frankfurt.de (R.P. Brandes).

https://doi.org/10.1016/j.yjmcc.2024.02.003
Received 11 December 2023; Received in revised form 15 January 2024; Accepted 6 February 2024
Available online 15 February 2024

hypertrophy [11] and deletion of the protein in myeloid cells promotes atherosclerosis [12]. In agreement with the repressive function of the protein, these studies collectively demonstrated that loss of NCoR1 promotes proliferation and hypertrophy.

Angiogenesis is the formation of new blood vessels by sprouting from the existing vasculature. It frequently occurs to promote oxygen and nutrient availability to an insufficiently supplied tissue [13]. Moreover, developmental conditions, regeneration and healing are associated with angiogenesis. Inadequate angiogenesis may lead to pathological cardiovascular states, such as microangiopathy [14]. In contrast, excessive angiogenesis is required for tumor growth, hence it is typical for neoplastic diseases such as cancer [15].

Endothelial cells are the main cell type involved in the primary angiogenic response [16]. Endothelial growth factors, such as vascular endothelial growth factor (VEGF), promote proliferation and migration upon receptor binding [17]. However, the angiogenic process is complex and certain aspects differ in a context-specific manner. An important aspect in sprouting angiogenesis is the selection of tip- and stalk cell subtypes in the endothelium [18]. Tip cells sense environmental cues and migrate towards a pro-angiogenic stimulus, while stalk cells follow and extend to build the sprout [19]. Tip- and stalk cell selection is a process controlled by Notch signaling. The Notch family consists of four members (NOTCH1, NOTCH2, NOTCH3, NOTCH4), of which Notch4 is mainly confined to endothelial cells, where it has context-dependent functions. Upon ligand binding, the membrane-bound Notch receptors undergo proteolytic cleavage, forming a Notch extra-cellular domain and a Notch intra-cellular domain (NICD). The extent of Notch signaling is dependent on ligand and receptor availability [20]. NICD translocates into the nucleus, where it binds to the transcription factor Recombination signal binding protein for immunoglobulin kappa J region (RBPJk), thereby removing the previously bound corepressor. Subsequently, coactivator proteins are recruited, converting the function of RBPJk from a repressive to an activatory transcriptional complex, promoting gene transcription [21,22].

These considerations suggest that nuclear corepressors limit the angiogenic response and hence might be a promising target to promote angiogenesis. In the present study, it was therefore determined which nuclear corepressor is most abundant in endothelial cells and most important for angiogenic function, including a characterization how it may control angiogenesis.

2. Materials and methods

2.1. Cell culture

Human umbilical vein endothelial cells (HUVECs), obtained from PromoCell (C-12203, Lot No. 405Z013, 408Z014, 416Z042), were cultured on fibronectin (1 mg/ml) coated dishes to passage 3 and used for experiments at passage 4. Endothelial growth medium (EGM, PeloBiotech) containing 8% FCS, 50 U/ml penicillin and 50 µg/ml streptomycin (Gibco) and growth factors (EGF, bFGF, IGF, VEGF, Heparin, L-Glutamin) was used as cell culture medium. In case of starvation, cells were cultured in endothelial basal medium (EBM) (PeloBiotech) containing 1% FCS, 50 U/ml penicillin and 50 µg/ml streptomycin (Gibco), EndoCGS-Heparin (PeloBiotech) at least 4 h prior to an experiment.

2.2. Animals

For this study NCoR1$^{flox/flox}$-CDH5-Cre*ERT2*$^{0/+}$ mice were used. These endothelial specific, tamoxifen inducible mice were generated by crossing NCoR1$^{flox/flox}$ mice [10] with Cdh5-CreERT2 (Tg(Cdh5-CreERT2)^{1Rha}) mice [23] (kindly provided by Ralf Adams, Münster, Germany). Endothelial NCoR1 deletion was induced by application of tamoxifen with the chow (400 mg/kg) for 10 days. Subsequently, tamoxifen free chow as “wash out” period of 14 days was given. In the present study, control animals are defined as NCoR1$^{flox/flox}$-CDH5-Cre*ERT2*$^{0/0}$ littermates, without cre-expression, which underwent the same tamoxifen treatment. All animals had free access to chow and water in a specified pathogen-free facility with a 12 h light/dark cycle and all animal experiments were performed in accordance with the German animal protection law and were carried out after approval by the local authorities (Regierungspräsidium Darmstadt, approval number FU1273). Every mouse received an identification number for each experiment and the experimenter was blind for the genotype. Animal group sizes differ due to number of available littermates.

2.3. Aortic Ring assay

The assay is an ex vivo method to study the angiogenic capacity of mouse aortic segments in organ culture by the quantification of endothelial sprouts. In brief, mice were killed by decapitation and the thoracic aorta was isolated, cleaned from fibro-adipose tissue and cut into 1 mm long rings. Subsequently, rings were embedded into a collagen gel and incubated with 2,5% autologous serum and 30 ng/ml $VEGF_{165}$ for up to 6 days. The culture medium was exchanged after 72 h. To differentiate between endothelial cells and fibroblasts, immunohistochemically staining of CD31 (1:200, BD BioSciences) was performed. For this, rings were washed with PBS and fixed with 4% PFA. Subsequently, the tissue was permeabilized and blocked with 0,5% Triton X-100 and 1% BSA overnight. Then, the primary antibody (1:200) was incubated overnight at 4 °C. After five washing steps with PBS, the tissue was incubated with the secondary antibody Alexa Fluor 647 (1:500, Invitrogen) overnight at 4 °C. Subsequently, the tissue was further fixed with 4% PFA for 10 min and store samples in the dark at 4 °C till image acquisition. Images were acquired with an Evos XL Core microscope (Life technologies). Analysis of cumulative sprout length and number was performed with ImageJ version 1.48. [24].

2.4. Whole mount en Face immunofluorescence staining

This staining of the aorta was performed to determine endothelial efficiency of NCoR1 knockout in NCoR1$^{flox/flox}$-CDH5-Cre*ERT2*$^{0/+}$ mice. The thoracic aorta was dissected, portioned into segments and cut open. Vessels were fixed in 4% PFA for 5 min followed by a permeabilization step with 1% BSA, 0.1% Triton X-100 and donkey serum for 30 min at RT. Subsequently, vessels were blocked for an additional 30 min in 1% BSA and donkey serum. Next, the aorta was then incubated with primary antibodies against NCoR1 (1:200, Cell Signaling) and CD31 (1:200, BD BioSciences) at 4 °C overnight, washed twice with 0.1% Tween in PBS followed by 2 washing steps with only PBS for 5 min each and then incubated with respective secondary antibodies for 30 min. Cell nuclei were stained with DAPI (1:200, Sigma Aldrich). Vessels were mounted in Dako Fluorescence Mounting medium (Agilent Technologies Inc.) and fluorescence images were acquired with a Zeiss LSM800 laser scanning microscope (Carl Zeiss Microscopy GmbH).

2.5. Protein isolation and Western blot analysis by SDS-PAGE

HUVEC were scraped into Hanks solution (Applichem), centrifuged down and subsequently lysed with RIPA buffer (1× TBS, 1% Desoxycholat, 1% Triton, 0.1% SDS, 2 mM Orthovanadat (OV), 10 nM Okadaic Acid (OA), protein-inhibitor mix (PIM), 40 µg/ml Phenylmethylsulfonylfluorid (PMSF)). Subsequently, benzonase (1:800) was added and samples were incubated for 15 min at 25 °C, followed by incubation for 60 min on ice. Next, samples were centrifuged (10 min, 16,000 xg), and protein concentrations of the supernatant were determined using the Bradford assay and the extract was boiled in Laemmli buffer. 50 µg of protein per sample were separated by SDS-PAGE. Next, gels were blotted onto a nitrocellulose membrane, which was blocked in Rotiblock (Carl Roth) for 30 min. After application of the primary antibody (Table 1), an infrared-fluorescent-dye-conjugated secondary antibody (Licor) was used. Signals were detected with an infrared-based

Table 1
Table of used antibodies with catalog numbers and companies.

Antibody	Catalog Number	Company
NCOR1	5948S	Cell Signaling
Actin, beta- (13E5)	4970S	Cell Signaling

laser scanning detection system (Odyssey Classic, Licor).

2.6. Proximity ligation assay (PLA)

The assay was performed using the Duolink In Situ Detection Reagents Orange Kit (#DU92007, Sigma Aldrich) according to the manufacturer's instructions. If necessary, knockdown was performed 24 h prior to the assay and HUVECs were grown to confluence in 8-well µ-ibidi slides. Next, cells were fixed using 4% PFA, followed by permeabilization using 0.05% Triton X-100 for 10 min. Blocking of cells was performed for 60 min using the Duolink BlockingSolution. Primary antibodies against NCoR1 (1:500, Cell Signaling) and RBPJk (1:500, Santa Cruz Biotechnology) were incubated overnight at 4 °C. The next day, cells were washed with washing buffer A and incubated at 37 °C with the provided anti-mouse MINUS and anti-rabbit PLUS PLA probes. Subsequently, enzymatic ligation was performed for 30 min at 37 °C followed by an amplification step using a polymerase for 100 min at 37 °C. Cells were washed with washing buffer B and cell nuclei were stained using DAPI. Fluorescence images were acquired using a Zeiss LSM800 laser scanning microscope (Carl Zeiss Microscopy GmbH).

2.7. siRNA transfection

HUVECs were seeded at a concentration of 20.000 cells/cm^2 and transfected on the following day in Endothelial basal medium containing 1% FCS using GeneTransII transfection reagent (MoBiTec) according to the manufacturer's instructions. Briefly, a final concentration of 60 nM siRNA (Table 2) together with GeneTrans II transfection reagent and DNA Diluent B was added to the cells for 4 h. Subsequently, the cell culture medium was replaced with EGM and changed again after 24 h. 48 h after transfection, cells were used for experiments as indicated.

2.8. Spheroid outgrowth assay

This method is used to determine the angiogenic capacity of endothelial cells cultured in 3D gels. If necessary, knockdown was performed 24 h prior to the assay. Subsequently, hanging drops were prepared by seeding 50.000 HUVECs per condition in EGM containing 20% methyl cellulose onto hydrophobic square dishes and culturing upside down overnight. Treatment was performed as indicated in the respective figure captions during spheroid formation. The next day, spheroids were washed once with PBS and then embedded into a collagen gel. Subgroups were treated with inhibitors or $VEGF_{165}$ (30 ng/ml). Images were acquired 20 h after embedding with an Evos XL Core microscope (Life technologies). Analysis of cumulative sprout length and number was performed with ImageJ version 1.48. [24]. In case of the compensatory sprouting assay to study the tip cell position, permanently color-labeled HUVECs by lentiviral particles coding for either CFP or YFP were used.

Table 2
Table of used siRNAs with Catalog-Numbers and Companies.

siRNA	Catalog Number	Company
CTL	#12935300	Invitrogen
siNCoR1	#HSS114352	Invitrogen
siSMRT	#HSS114356	Invitrogen
siREST	#HSS109177	Invitrogen
siRBPJ	#HSS142633	Invitrogen

2.9. Tube formation assay

The method determines the angiogenic capacity of endothelial cells, by analyzing capillary-like structures. If necessary, knockdown was performed 48 h prior to the assay. 50 µl Matrigel (Corning) per well were added into a 96 well plate and allowed to polymerize for 30 min at 37 °C. Subsequently, 15.000 HUVECs were seeded onto the Matrigel and incubated in EBM with 1% FCS for 4 h at 37 °C. Next, cells were fixed using 4% PFA and images were acquired immediately using an Evos XL Core microscope (Life technologies). Number of junctions, tubuli and total branching length was determined using ImageJ version 1.48. [24].

2.10. Quantitative RT-qPCR

HUVECs were grown to confluence and treated as indicated. If necessary, knockdown was performed 48 h prior to the assay. For RNA isolation, the RNA Mini Kit (Bio&SELL) was used according to the manufacturer's instructions. For reverse transcription, RNA (500 ng) was mixed with oligo dT primers (Sigma-Aldrich, #O4387) and random hexamer (Sigma-Aldrich, #O4387) and subsequently reverse transcribed into cDNA using the SuperScript III reverse transcriptase (Thermo Fisher), 5× buffer (Thermo Fischer) and DTT (Thermo Fischer) according to the manufacturer's protocol. Quantitative real-time PCR was performed in an AriaMX Cycler (Agilent) with SYBR Green Master Mix (Bio&SELL) using to the comparative C_T quantitation method $2^{-\Delta\Delta Ct}$ with ROX (Bio&SELL) as a reference dye. GAPDH served as a housekeeping gene. Data were analyzed using the AriaMX qPCR software (Agilent). (See Table 3.)

2.11. RNA sequencing

RNA was isolated using the RNA Mini Kit (Bio&SELL). To avoid contamination by genomic DNA, samples were subjected to on-column DNase digestion (DNase-Free DNase Set, Qiagen). Total RNA and library integrity were verified on LabChip Gx Touch 24 (Perkin Elmer). Approximately 900 ng of total RNA was used as input for SMARTer Stranded Total RNA Sample Prep Kit - HI Mammalian (Takara Bio). Sequencing was performed on the NextSeq500 instrument (Illumina) using v2 chemistry with 1x75bp single end setup. Trimmomatic version 0.39 was employed to trim reads after a quality drop below a mean of Q20 in a window of 20 nucleotides and keeping only filtered reads longer than 15 nucleotides [25]. Reads were aligned versus Ensembl human genome version hg38 (Ensembl release 99) with STAR 2.7.3a. [26]. Aligned reads were filtered to remove duplicates multi-mapping, ribosomal, or mitochondrial reads with Picard 2.21.7 (Picard: A set of tools (in Java) for working with next generation sequencing data in the

Table 3
Table of used forward and reverse primers.

Primer Name	Forward (5′ - 3`)	Reverse (3`- 5`)
NCOR1	TCCTGTGGAGCAGAAACACC	TCATCACCTGGTTTGTCTTGA
SMRT	CACGAGGTGTCAGAGATCATCG	GCCATAAGCCCGTTCATGTTG
REST	CGGTTGGGGATAACAACTTTTCA	TCTACGACGCTGAGTTCCAAA
VCAN	GTAACCCATGCGCTACATAAAGT	GGCAAAGTAGGCATCGTTGAAA
VEGFR1	GGAAGGCATGAGGATGAGAG	CAGAGAAGGCAGGAGTTGAG
VEGFR2	GGGAGTCTGTGGCATCTGAAGG	GAGAATCTGGGCTGTGCTACCG
VEGFR3	GGTACATGCCAACGACACAG	GTTGACCAAGAGCGTGTCAG
MMP10	TTTGGCTCATGCCTACCCAC	TCTTGCGAAAGGCGGAACTG
TGFBR1	ACGGCGTTACAGTGTTTCTG	GCACATACAAACGGCCTATCTC
NOTCH1	CAGGCAATCCGAGGACTATG	CAGGCGTGTTGTTCTCACAG
NOTCH2	TGGTGGTCAGTGCATGGATAG	ATCTGGGGACACACATCGAC
NOTCH4	CGAGGAAGATACGGAGTGGC	CTGCTCTGGTGGGCATACAT
DLL4	CAGCACTCCCTGGCAATGTA	CACAGTAGGTGCCCGTGAAT
HEY1	GCCAGCATGAAGCGAGCTC	GGGTCAGAGGCATCTAGTCC
HEY2	AGATGCTTCAGGCAACAGGG	CTGAATCCGCATGGGCAAAC
GAPDH	TGCACCACCAACTGCTTAGC	GGCATGGACTGTGGTCATGAG

BAM format; https://broadinstitute.github.io/picard/, accessed 2023-12-08). Gene counts were established with featureCounts 1.6.5 by aggregating reads overlapping exons on the correct strand excluding those overlapping multiple genes [27]. The raw count matrix was normalized with DESeq2 version 1.26.0. [28]. Contrasts were created with DESeq2 based on the raw count matrix. Genes were classified as significantly differentially expressed at average count >5, multiple testing adjusted *p*-value <0.05, and − 0.585 < log2FC > 0.585. The Ensemble annotation was enriched with UniProt data (Activities at the Universal Protein Resource (UniProt)) [29].

2.12. ATAC sequencing

25000 FACS-sorted cells were collected by centrifugation at 1000 *g* for 5 min and used for ATAC Library preparation using Tn5 Transposase from Nextera DNA Sample Preparation Kit (Illumina). The cell pellet was resuspended in 50 µl Lysis/Transposition reaction (12.5 µl THS-TD-Buffer (Tris-acetate, pH 7.8 132 mM, Potassium acetate (Sigma, 95843-100ML-F) 264 mM, Magnesium acetate (Sigma, 63052-100ML) 40 mM, Dimethylformamide (DMF) (Sigma, Sigma D4551-250ML) 64%, H2O), 2.5 µl Tn5, 5 µl 0.1% Digitonin and 30 µl water) and incubated at 37 °C for 30 min with occasional snap mixing. DNA fragments were purified using the MinElute PCR Purification Kit (Qiagen). Amplification of library together with indexing primers was performed as described elsewhere [30]. Libraries were mixed in equimolar ratios and sequenced on NextSeq2000 platform with 2x36bp paired-end setup. Reads were aligned to the human genome (GRCh38.p13) using Bowtie2 (v2.4.5) [31] with the parameter –very-sensitive. Duplicates were removed and files were indexed using samtools (v1.10) [32] Normalized read coverage was computed using DeepTools bamCoverage (v3.5.1) [33], so that ATAC signal could be viewed in a genome browser. Peaks were called from the data using MACS3 (v3.0.0) [34] with the parameters –scale-to-small and –format BAMPE. Regions of the genome changed in their accessibility were also identified using MACS3, this time using the bdgdiff functionality to compute log-likelihood ratios between siScr and siNCOR1 ATAC-sequencing coverage in peak regions.

2.13. TEPIC analysis

TEPIC is a segmentation-based method to predict transcription factor (TF) binding in open chromatin regions [35]. In this analysis, peak calling and identification of differentially accessible peaks was performed on the ATAC-seq data as previously described. Next, TEPIC 2 was applied to compute predicted TF binding affinities in peak regions increased in accessibility following siNCOR1. In a gene-focused analysis, transcription factors which were predicted to bind in regions of differentially accessible chromatin around differentially expressed genes were of particular interest, and so transcription factors expressed in HUVEC with predicted affinity in these regions were identified from the TEPIC results. Predicted binding was compared to true transcription factor binding sites for JUN and HEY1 through the use of ChIP-sequencing data from the ENCODE project [36].

2.14. Expression analysis

Expression of corepressors across all cells, log-normalized *NCOR1* expression in endothelial cells and *NCOR1* expression in different vessel types, originating from different organs was analyzed in the scRNA-sequencing compenium *Tabula Sapiens*. [37]. Normalized expression of NCoR1 in murine endothelial cells and scaled expression of NCoR1 in mouse vascular cells was analyzed using Tabula muris [38]. Differential enrichment analysis of genes changed after *NCOR1* knockdown was achieved using Wikipathway [39].

2.15. Proliferation assay

HUVECs were seeded in triplicates onto 96 well ImageLock plate at a density of 1.500 cells/well. If applicable, knockdown was performed 24 h prior to the assay. Cells were allowed to settle for 4 h. Subsequently, cell culture medium was exchanged and cells were labeled with Incucyte Nuclight Rapid Red Dye (1:1000). The ImageLock plate was placed in the live-cell imaging Incucyte system. Images were acquired every 3 h for a total period of 100 h using the red imaging channel. Analysis was performed with the Incucyte software, thereby quantifying the number of cells over time.

2.16. Migration Scratch wound assay

HUVECs were seeded in triplicates onto a 96 well ImageLock plate at a density of 40.000 cells/well. If applicable, knockdown was performed 24 h prior to the assay. Cells were allowed to settle for 24 h. The cellular monolayer was scraped in the center of the well in a straight line using a Scratch wound maker (SatoriusAG) and the media was immediately replaced with fresh EGM. The ImageLock plate was placed in the live-cell imaging Incucyte system. Images were acquired every 1 h for a total period of 16 h using the phase contrast imaging. Analysis was performed with the Incucyte software, thereby quantifying relative wound closure over time.

2.17. Directed migration assay

HUVECs were seeded on fibronectin (Sigma Aldrich) coated 8-well ibiTreat µ-slides (ibidi GmbH) 48 h after transfection. The gradient of 0%–20% FCS was applied 2 h after seeding. Immediately after, live cell tracking was performed using the Cell Observer microscope (Zeiss) at 37 °C and 5% CO2 for 20 h with pictures taken every 10 min. Analysis of cell migration was performed using the ImageJ Software (Chemotaxis and Migration Tool) with 30 cells tracked per condition.

2.18. Statistical analysis

All experiments were independently performed at least three times as indicated by the number (n) in the respective figure legend. Statistical analysis was performed using Prism 8.3.0. ANOVA followed by Tukey's test or student *t*-test was used to evaluate statistical significance. Values of $P \leq 0.05$ were considered significant. All data are expressed as mean ± standard error of mean (SEM).

3. Results

3.1. NCoR1 is the most abundant nuclear corepressor in endothelial cells

The human genome codes for more than >25 nuclear repressors. In order to identify the most relevant ones, their expression was determined from the Tabula Sapiens single cell RNA sequencing (scRNA-seq) data set [37]. Aggregated expression was highest for 'nuclear receptor corepressor 1' (*NCOR1*), followed by 'ligand-dependent corepressor' (*LCOR*) and 'silencing mediator of retinoid and thyroid hormone receptors' (*NCOR2 / (SMRT)*) (Fig. 1A). Of all vascular cell types resolved in Tabula Sapiens, endothelial cells exhibited the broadest *NCOR1* expression (Fig. 1B) Thereby, *NCOR1* expression stays constant across endothelial cells originating from different organs or different vessel types (Supplementary Fig. S1.). Bulk RNA-seq data from human umbilical vein endothelial cells (HUVEC) was also analyzed to verify these findings in cultured cells. Here, *NCOR1* was the highest expressed nuclear corepressor (Fig. 1C). In accordance with the scRNAseq data, *SMRT*, *REST* (RE-1 silencing transcription factor) and *LCOR* expression were similar. To more specifically analyze the vascular compartment, data from Tabula Sapiens (Fig. 1D-F) and Tabula Muris [38] (Fig. 1G-I) were reclustered for vascular cells and analyzed with respect to

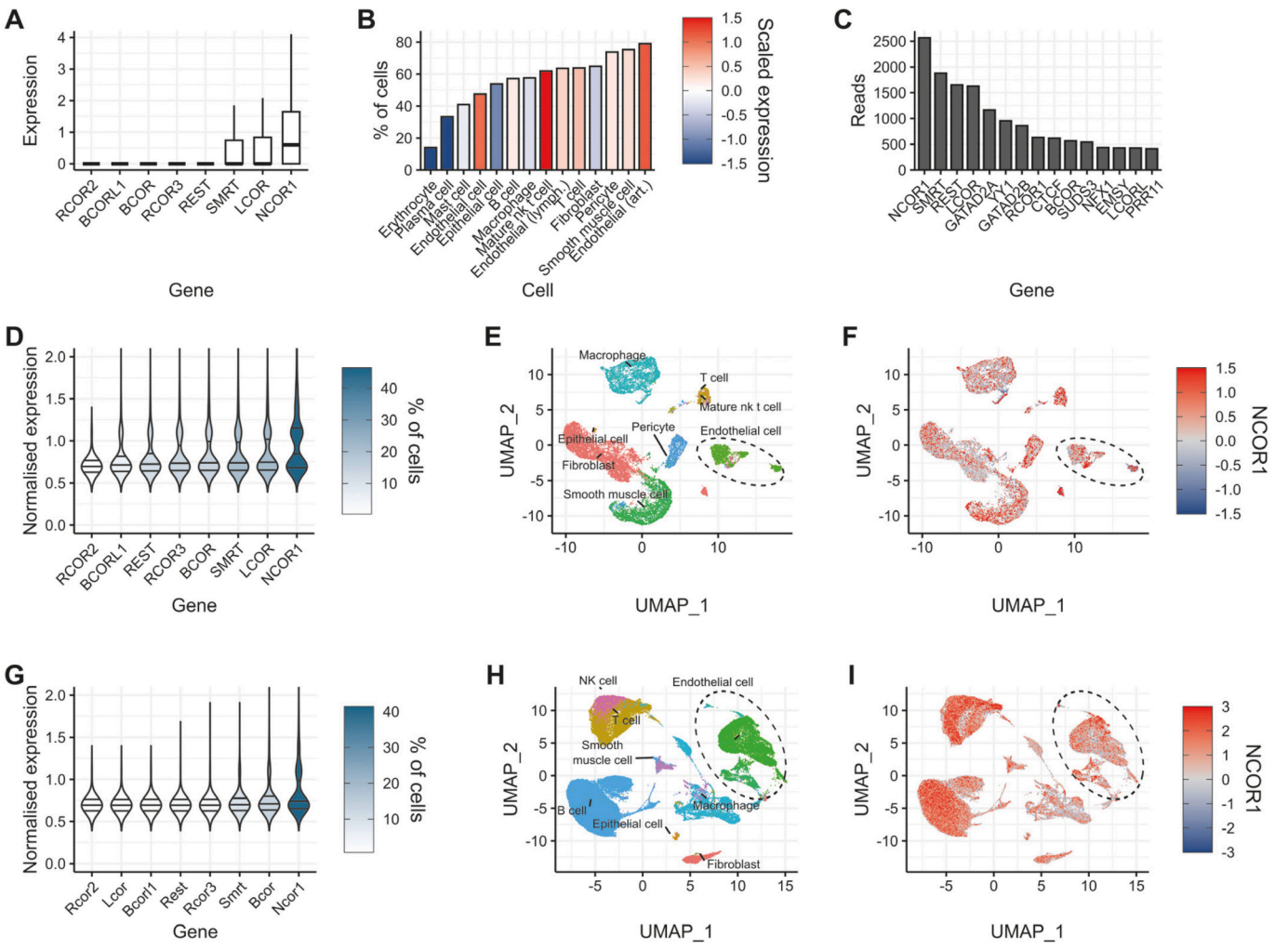

Fig. 1. *NCOR1* is the most abundant nuclear repressor in endothelial cells.
(A) Expression of corepressors across all cell types in Tabula Sapiens. **(B)** Percentage of cells expressing NCOR1 and scaled expression per cell type of the vasculature in Tabula Sapiens. **(C)** Mean expression of repressors in HUVEC determined by RNA-seq. **(D)** Normalized expression of corepressors in human endothelial cells. **(E)** *Re*-clustering of vascular cells present in Tabula Sapiens. **(F)** Scaled *NCOR1* expression across human vascular cell types. **(G)** Normalized expression of *Ncor1* in murine endothelial cells. **(H)** *Re*-clustering of cells of the mouse vasculature present in Tabula Muris. **(I)** Scaled expression of *Ncor1* in mouse vascular cells.

repressor expression. Also with this approach, *Ncor1* was ubiquitously expressed across the vasculature and exhibited a particular high expression in endothelial cells (Fig. 1 D—I).

3.2. NCoR1 limits endothelial angiogenic function

Having identified the highest expressed corepressors in endothelial cells, their contribution to angiogenic function was tested using a knockdown strategy. siRNA treatment of HUVEC achieved sufficient knockdown of *NCOR1*, *SMRT* and *REST* (Supplementary Fig. S2). In the matrigel tube formation assay, knockdown of *NCOR1* increased number of junctions and tubuli, whereas that of *SMRT* and *REST* did not (Fig. 2A&B). Endothelial angiogenic sprouting in the spheroid outgrowth assay under basal conditions was also increased, and this effect was mediated by both an increased sprout length and sprout number (Fig. 2C&D). VEGF stimulated the angiogenic response in all groups, but the relative potency of this effect was significantly attenuated in the NCoR1-depleted groups (Fig. 2C&D). To study whether the pro-angiogenic effect of NCoR1 depletion was a consequence of increased proliferation and migration, these aspects were determined separately using the Incucyte automated cell imaging system. Migration in response to scratch application as well as proliferation in response to a combination of growth factors and medium were, however, not elevated. Both responses were in fact decreased by knockdown of *NCOR1* (Fig. 2E&F). The observed differences between 2D- and 3D-cell culture systems can be consequence of a different matrix composition but also different receptor-dependent signaling. To further define the nature of the underlying difference, directed migration was determined in 2D cell culture. Migration velocity and migrated distance was not affected by siRNA-mediated knockdown of *NCOR1,* but forward migration, and thus directionality, was significantly attenuated. These findings suggest that the ability of cells to sense or react to growth factor gradients is specifically attenuated after *NCOR1* knockdown. (Fig. 2G&H). The basal migratory capacity, in contrast, appears to increase when *NCOR1* expression is attenuated in endothelial cells.

3.3. NCOR1 knockdown induces a pro-angiogenic gene signature

To explore the mechanistic basis of the pro-angiogenic effect of *NCOR1* knockdown, RNA-seq was performed. Knockdown efficiency was validated by Western Blot analysis, showing a reduction by 73% in NCoR1 protein expression (Fig. 3A, Supplementary Fig. S7.). The principal component analysis highlights the impact of siRNA-mediated knockdown of *NCOR1*, albeit a strong impact of each individual replicate (Fig. 3B). In response to *NCOR1* knockdown 991 genes were differentially expressed (523 up, 468 down, Fig. 3D) Among the top 50

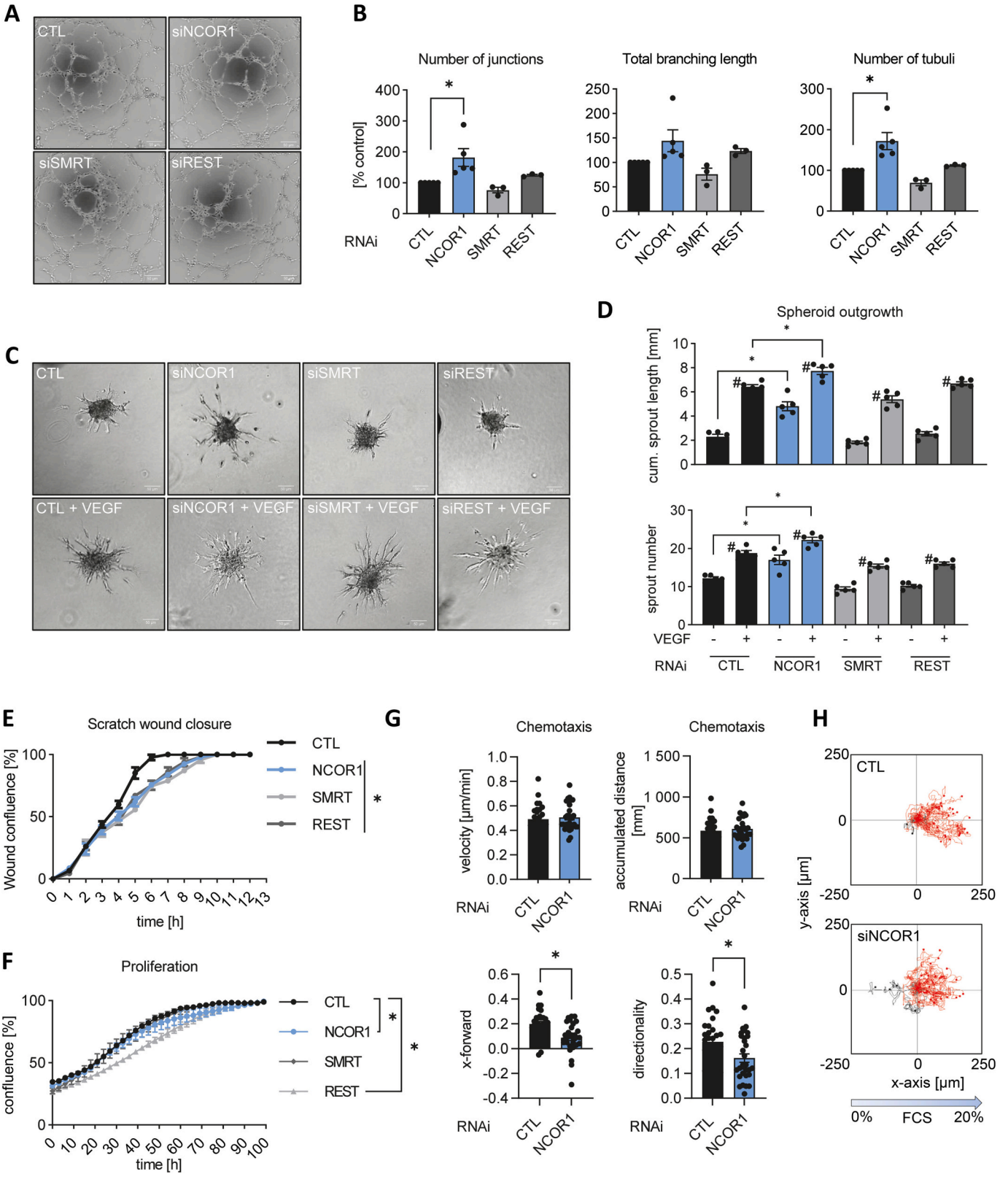

(caption on next page)

Fig. 2. NCoR1 limits endothelial angiogenic function.
(A&B) Tube formation assay of HUVECs after siRNA-mediated knockdown of *NCOR1*, *SMRT* or *REST*. Scrambled siRNA served as negative control (CTL). Representative images **(A)** and quantification of number of junctions, total branching length and number of tubuli are shown **(B)**. n = 3, One-way ANOVA. $^{*}P < 0.05$. **(C&D)** Spheroid outgrowth assay of HUVECs after siRNA-mediated knockdown of *NCOR1*, *SMRT* or *REST*. Scrambled siRNA served as negative control (CTL). Spheroids treated with or without VEGF-A are shown. Representative images **(C)** and quantification of cumulative sprout length and sprout number per spheroid **(D)**. n = 5, One-way ANOVA. $^{*}P \leq 0.05$ vs. CTL. $^{\#}P \leq 0.05$ CTL vs. VEGF. **(E)** Scratch wound assay of HUVECs after siRNA-mediated knockdown of *NCOR1*, *SMRT* or *REST*. Scrambled siRNA served as negative control (CTL). Quantification of relative wound closure over time is shown. n = 3, One-way ANOVA of Area under the curve (AUC). $^{*}P < 0.05$. **(F)** Proliferation assay of HUVECs after siRNA-mediated knockdown of *NCOR1*, *SMRT* or *REST*. Scrambled siRNA served as negative control (CTL). Quantification of total nuclei over time was measured and displayed as confluence (%). n = 3, One-way ANOVA of Area under the curve (AUC). $^{*}P < 0.05$. **(G-H)** Directed migration assay of HUVECs after siRNA-mediated knockdown of *NCOR1*. Scrambled siRNA served as negative control (CTL). Migration was determined by live cell tracking for 20 h and quantified by using ImageJ. A total of 30 cells per condition were analyzed regarding velocity, accumulated distance, x-FMI and directionality n = 3, Unpaired *t*-test. $^{*}P < 0.05$. Statistics **(G)** and tracking **(H)** are of the individual conditions.

differentially regulated genes numerous ones associated with angiogenesis and of those *JAG1*, *ADAMTS4*, *ANGPT2*, *ITGAV* were induced (Fig. 3C). In fact, gene ontology analysis with Wikipathway returned VEGF signaling and neovascularization as significantly enriched terms, supporting the notion that knockdown of *NCOR1* induces a growth factor-independent angiogenic response (Fig. 3E). To focus the analysis towards this search space, the genes contained in the GO-term "angiogenesis" were reclustured (Fig. 3F); which indeed were almost exclusively upregulated in response to knockdown of *NCOR1*. In line with this, a transcription factor enrichment analysis of the promoters of the differentially regulated genes returned HIF1α and EGR1, which all contribute to angiogenesis (Fig. 3G).

In order to address whether the angiogenic gene signature has a certain specifity to *NCOR1* knockdown and to confirm the RNA-seq data, the differential expression of a few prominent genes was confirmed by RT-qPCR in HUVEC (Fig. 3H). This not only confirmed that knockdown of *NCOR1* results in an increased expression of *VCAN*, *FLT1, KDR, FLT4, MMP10 and TGFBR1*, it also showed that neither *SMRT* nor *REST* knockdown could mimic this effect. It should however be noted, that *SMRT* knockdown increased *FLT1* and *FLT4*, albeit to a lesser extent (Fig. 3H). Collectively, these data support our concept that that knockdown of *NCOR1* induced a growth factor-independent, pro-angiogenic signature in endothelial cells.

3.4. Knockout of NCoR1 promotes angiogenic function of the mouse aorta in organ culture

In order to determine whether the pro-angiogenic response of NCoR1 depletion is also present in naïve endothelial cells in the vascular context, tissue of tamoxifen-inducible, endothelial-specific NCoR1 knockout mice (NCoR1$^{flox/flox}$-Cdh5-Cre*ERT2*$^{0/+}$) was studied. Control animals, which are defined as NCoR1$^{flox/flox}$-CDH5-Cre*ERT2*$^{0/0}$ littermates, without Cre-recombinase expression, underwent the same treatment. The efficiency of in vivo tamoxifen application for the NCoR1 knockout was determined in the aorta by *en face* staining. Aortic endothelial NCoR1 expression is high and activation of the Cre-recombinase resulted essentially in a complete loss of endothelial NCoR1 staining (Fig. 4A). Functionally, endothelial cell outgrowth was determined in aortic organ culture (Fig. 4B). Similarly, to the previously described spheroid outgrowth assay, loss of NCoR1 promoted endothelial angiogenic function. The effect, which was primarily mediated by an increase in sprout number, was already observed under basal conditions and therefore VEGF-independent (Fig. 4C). Collectively, these data suggest that loss of NCoR1 results in the de-repression of an angiogenic program. Whether the increased sprouting is, however, a receptor-mediated effect or a dedifferentiation phenomenon is unclear.

3.5. Depletion of NCoR1 leads to genome-wide chromatin opening, including at angiogenic gene promoters

To address the aspect of VEGF-dependency, a pathway specific inhibitor (KRN633) was used that attenuated spheroid outgrowth in response to VEGF in CTL siRNA transfected cells. In contrast to this, it did not impact the *NCOR1* siRNA-stimulated spheroid outgrowth (Supplementary Fig. S3). This suggests that the classic VEGF-dependent pathway is not mediating the effect of *NCOR1* siRNA-mediated knockdown.

Nuclear receptor corepressors mediate their function by recruitment of histone deacetylases, which mediate the deacetylation of histones, a process required for chromatin closure [40]. Due to the distance between NCoR1 and the DNA and the fact that recruitment is context dependent, chromatin immunoprecipitation and sequencing (ChIP-seq) to identify NCoR1-DNA interaction is not feasible. To explore the relationship between NCoR1-dependent gene expression and chromatin conformation, ATAC-seq (assay for transposase-accessible chromatin) was performed, which uses transposase-accessibility to identify open and therefore accessible chromatin areas. ATAC-seq was performed in HUVEC treated with either scrambled siRNA or siRNA targeted against the *NCOR1* transcript (Fig. 5A). Knockdown of *NCOR1* in HUVEC significantly changed chromatin accessibility in a genome-wide manner, with an expected dramatic increase in chromatin accessibility (Fig. 5B). This effect was particularly strong for promoter regions as compared to other genomic features (UTRs, introns, exons, intergenic) (Fig. 5C). In order to determine whether the effect was also observed for angiogenesis-associated genes, several were manually inspected and H3K4me3 ChIP-sequencing was overlayed to mark promoter regions (Fig. 5D-G, Supplementary Fig. S4). Indeed, knockdown of *NCOR1* also increased promoter accessibility of angiogenesis-associated genes.

Binding of transcription factors limits transposase-accessibility and therefore ATAC-seq can be used to infer transcription factor binding, with the aid of the TEPIC tool. TEPIC allows the prediction of transcription factor binding affinity in regions of open chromatin associated with genes [41]. Among transcription factors receiving a high TEPIC score were JUN, FOSL2, FOSL1, BACH1 and HEY1 and HES2 (Fig. 5H). In order to validate these predictions, ChIP-sequencing data from the ENCODE project for JUN (number 1 hit) and HEY1 were analyzed. For integrin αV (gene ITGAV), which was induced upon *NCOR1* siRNA treatment, a HEY1 peak and multiple JUN binding sites lining up with altered chromatin accessibility could be identified (Fig. 5I). HEY1 is known to be a direct target gene of Notch signaling [42], while the JUN family, especially JunB, has previously been linked to endothelial sprouting, with an especially high expression in tip cells [43].

3.6. Knockdown of NCOR1 results in endothelial tip cell specification

To study whether *NCOR1* knockdown actually promotes tip-cell like behavior, a modified spheroid outgrowth assay was performed. HUVECs were permanently color-labeled by lentiviral particles coding for either Cyan-Fluorescent-Protein (CFP) or Yellow-Fluorescent-Protein (YFP). The specifically colored cells were transfected with either NCoR1 siRNA (siNCOR1) or scramble siRNA (siCTL) and subsequently, mixed spheroids of both conditions were formed. Due to the color coding, *NCOR1* knockdown and control cells could be discriminated in the spheroid. For the analysis of the tip cell, the color of the cell in the leading position of the tip was identified. The tip position was an NCoR1 siRNA treated cell in 74% of the sprouts, leaving only 26% of tips where a control cell was

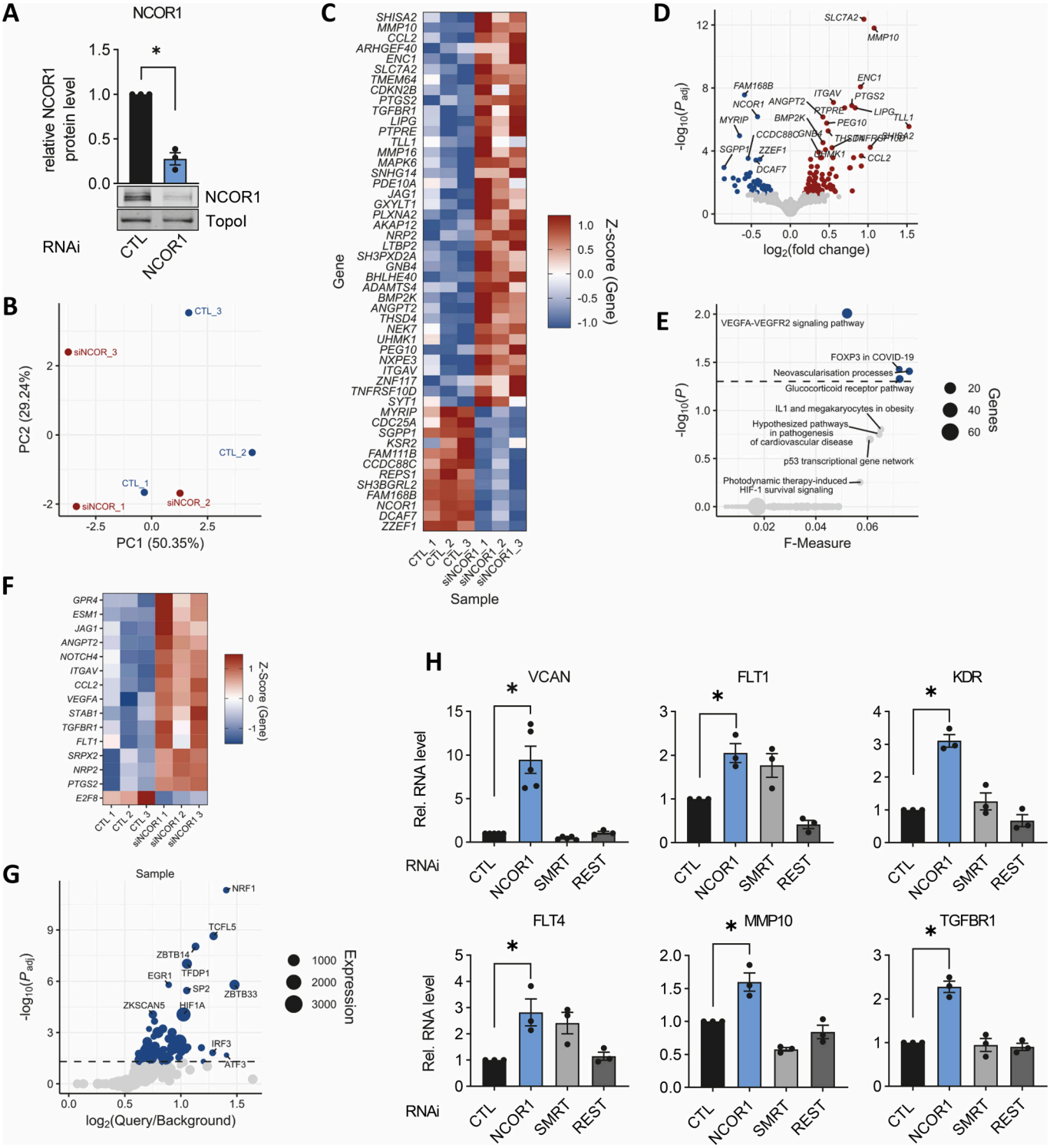

Fig. 3. *NCOR1* knockdown induces an angiogenic signature.

(A) Western Blot analysis of NCOR1 (NCOR1) and Topoisomerase (TopoI) with and without siRNA-mediated knockdown of NCOR1 from HUVECs. Scrambled siRNA served as a negative control (CTL). n = 3. One-way ANOVA. $*P < 0.05$ **(B)** PCA plot of sequenced samples from control and *NCOR1* knockdown conditions. n = 3 **(C)** Top 50 differentially expressed genes after *NCOR1* knockdown from HUVECs, normalized by *Z*-score and hierarchically clustered. **(D)** Volcano plot of differential gene expression analysis. Red indicates upregulation in response to *NCOR1* knockdown. **(E)** Wikipathway enrichment analysis of genes differentially expressed following *NCOR1* knockdown from HUVECs. **(F)** Gene expression of the differentially expressed genes of the GO-term angiogenesis in response to *NCOR1* knockdown from HUVECs. **(G)** Transcription factor motif enrichment analysis in promoters of genes differentially regulated after *NCOR1* knockdown, versus genomic background. **(H)** RT-qPCR of *VCAN*, *VEGFR1*, *VEGFR2*, *VEGFR3*, *MMP10*, *TGFBR1* after siRNA-mediated knockdown of *NCOR1*, *SMRT* or *REST* from HUVECs. Scrambled siRNA served as a negative control (CTL). n = 3. One-way ANOVA. $*P < 0.05$.

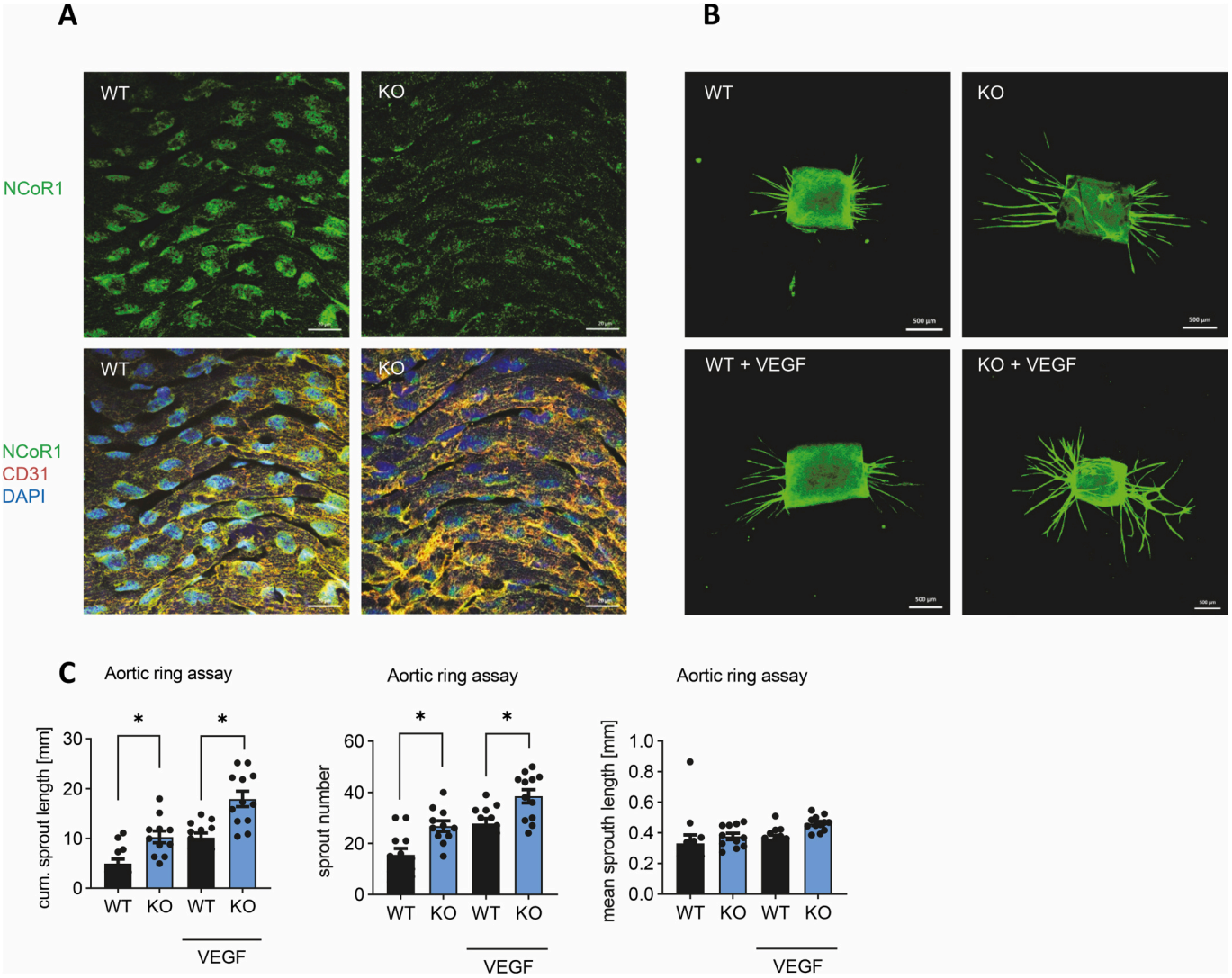

Fig. 4. Knockout of NCoR1 promotes angiogenic function of the mouse aorta in organ culture.
(A) En Face immunofluorescence staining of aorta from NCoR1$^{flox/flox}$-Cdh5-Cre*ERT2*$^{0/+}$ mice with and without tamoxifen-induced knockout for NCoR1 (green) and CD31 (orange). DAPI (blue) was used to counterstain the nuclei. Scale bars indicate 20 μm. **(B)** Aortic rings from NCoR1$^{flox/flox}$-Cdh5-Cre*ERT2*$^{0/+}$ mice with and without tamoxifen induced knockout. CD31 staining was used to visualize endothelial cells. Representative images of aortic rings treated with or without VEGF-A are shown. Scale bars indicate 500 μm. **(C)** Quantification of cumulative sprout length, sprout number per ring and mean sprout length. n = 12, One-way ANOVA. *$P < 0.05$.

present (Fig. 6A). This demonstrates that knockdown of *NCOR1* favors tip cell specification.

Tip cell specification can be linked to Notch signaling, one of the main pathways involved in the tip- and stalk-cell selection process [44]. Therefore, the role of Notch signaling was directly tested for spheroid outgrowth. Stimulation of Notch signaling by the Notch ligand Delta-like 4 (DLL4) [45], as expected, greatly attenuated spheroid outgrowth. Importantly, this effect was maintained after *NCOR1* knockdown (Fig. 6B). This demonstrates that *NCOR1* knockdown cells express Notch receptors and exhibit functional Notch signaling. Similarly, inhibition of Notch signaling by the γ-secretase inhibitor Dibenzazepine (DBZ) promoted spheroid outgrowth. The effect was more pronounced in control cells than in *NCOR1* knockdown cells, which might be due to the already high angiogenic activity in the latter cells (Fig. 6C).

To substantiate these findings, Notch gene expression was analyzed. NCoR1-depleted cells show elevated gene expression levels of *NOTCH1*, *NOTCH2*, *NOTCH4* as well as Notch target genes, like *DLL4*, *HEY1* and *HEY2*. SMRT or REST depletion failed to mimic the effects in a similar manner (Fig. 6D). Similar to the spheroid outgrowth assay, these effects can be blocked with DBZ (Supplementary Fig. S5). To address how NCoR1 may regulate Notch signaling, we performed a proximity ligation assay of NCoR1 and RBPJk, the main transcription factor of the Notch signaling pathway. A strong interaction between NCoR1 and RBPJk could be shown mainly in the nucleus of endothelial cells, which was sensitive to *NCOR1* knockdown, showing a reduced interaction the NCoR1-depleted condition (Fig. 6E&F). In agreement with these findings, we were able to show that this reduced interaction directly results in an increased RBPJk promotor activity (Fig. 6G). To further study the interaction between NCoR1 and RBPJk, we performed targeted knockdown of *RBPJk* itself (Supplementary Fig. S2), as well as combined knockdown of *NCOR1 and RBPJk*. A spheroid outgrowth assay revealed that in control cells RBPJk-depletion has little effect on sprouting but blocks the hypersprouting effect elicited by siRNA-mediated knockdown of *NCOR1* (Fig. 6H). These data suggest that loss of NCoR1 de-represses RBPJk-dependent gene expression, apparently by a Notch-dependent pathway. The latter is surprising given that Notch1 is reported to limit proliferation. We therefore hypothesized that another Notch member,

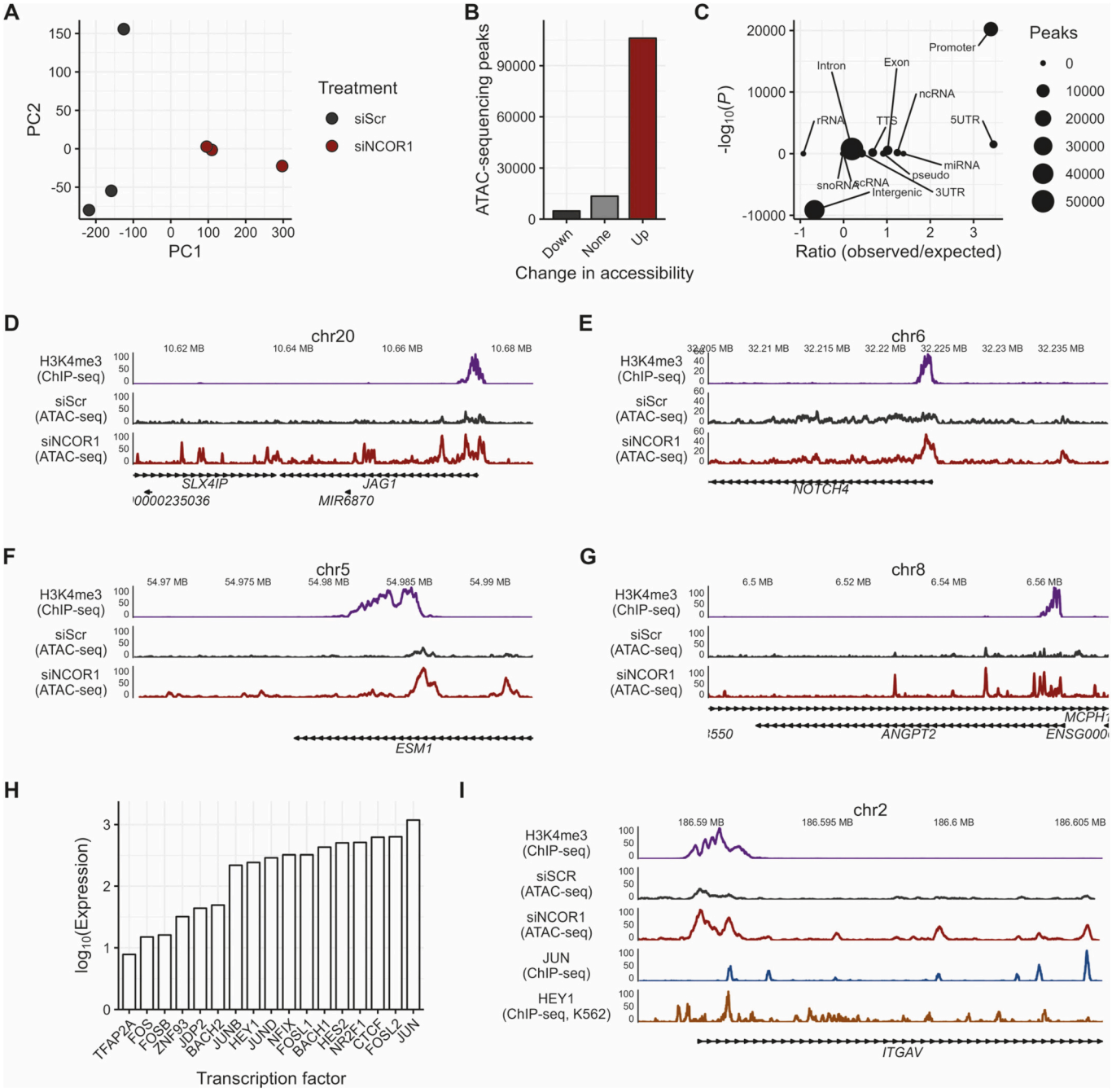

Fig. 5. Depletion of NCoR1 leads to genome-wide chromatin opening.
(A) Principal component analysis of ATAC-sequencing from HUVEC treated with either scrambled siRNA (siScr) or NCOR1 siRNA (siNCOR1). **(B)** Total numbers of differential ATAC-sequencing peaks between siNCOR1 and siScr. **(C)** Enrichment analysis grouped by genomic features as indicated. **(D-G)** Normalized ATAC-sequencing for the genes indicated comparing siScr and siNCOR1. H3K4me3 ChIP-sequencing data from HUVEC (ENCODE) are include to allow identification of promoter regions. **(H)** Expression of transcription factors predicted by TEPIC to bind in ATAC-sequencing peaks close to at least 75% of differentially regulated angiogenic genes identified in RNA-sequencing following siNCOR1. **(I)** ATAC-sequencing of ITGAV comparing siSCR and siNCOR1. JUN, HEY1 and H3K4me3 traces as obtained from ENCODE are overlayed.

potentially Notch4, which is also induced by *NCOR1* knockdown, might be responsible for the observed effect. This hypothesis was based on the fact that Notch4 can act as an endogenous inhibitor of Notch1, when both receptors are expressed in *cis* [46]. To study this, siRNA against *NOTCH1* or *NOTCH4* was applied with or without *NCOR1* suppression by siRNA and spheroid outgrowth was studied (Fig. 6I). *NOTCH1* knockdown slightly increased spheroid outgrowth, whereas *NOTCH4* knockdown slightly decreased it. In *NCOR1* knockdown cells, additional knockdown of *NOTCH1* had little effect. Importantly, and in contrast, *NOTCH4* knockdown blocked the stimulatory effect of *NCOR1* knockdown. In the presence of both knockdowns, sprouting was similar to control-transfected cells (Fig. 6I). This suggests that the pro-angiogenic effect of NCoR1 is mediated, at least in part, by the induction of *NOTCH4* and increased Notch4 signaling via its interaction with RBPJk.

4. Discussion

In the present study, we analyzed the contribution of nuclear

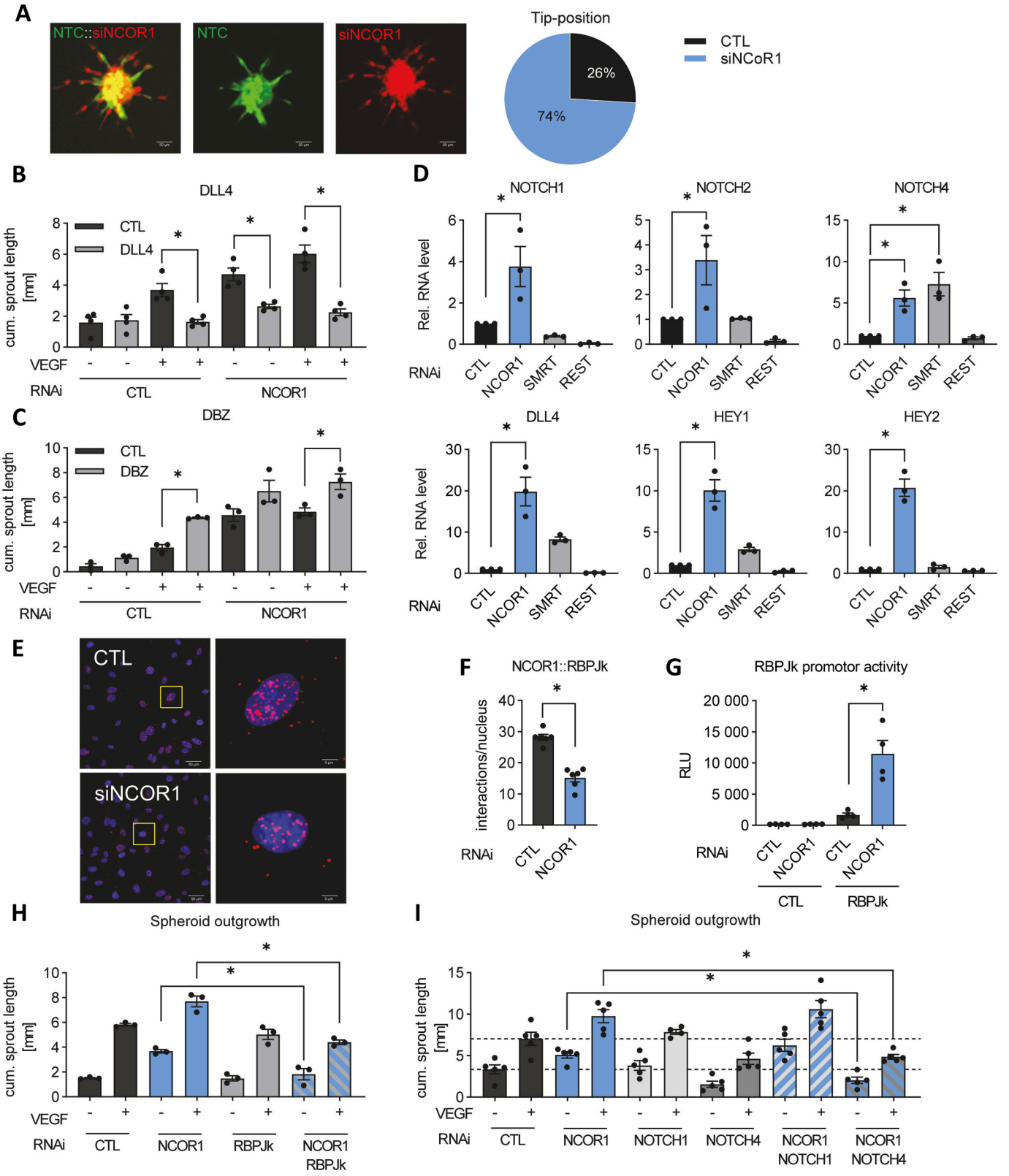

(caption on next page)

Fig. 6. Knockdown of *NCOR1* results in endothelial tip cell specification.
(A) Spheroid outgrowth assay of *NCOR1* depleted (red) and scrambled siRNA (green) HUVECs. Scrambled siRNA served as negative control (CTL). Quantification of tip cells per spheroid is shown. n = 3, Unpaired *t*-test. **(B&C)** Spheroid outgrowth assay of HUVECs after siRNA-mediated knockdown of NCOR1 or scrambled siRNA treatment (CTL). Spheroids were also treated as indicated with or without VEGF-A. Quantification of cumulative sprout length per spheroid is shown. n = 3, One-way ANOVA. $*P < 0.05$. **(D)** RT-qPCR of *NOTCH1*, *NOTCH2*, *NOCTH4*, *DLL4*, *HEY1* and *HEY2* after siRNA-mediated knockdown of *NCOR1*, *SMRT* or *REST* from HUVECs. Scrambled siRNA served as a negative control (CTL). n = 3. One-way ANOVA. $*P < 0.05$. **(E-G)** Duolink proximity ligation assay for NCOR1-RBPJk from HUVECs. Red signal indicates duolink PLA signal (546 nm), blue indicates DAPI. Representative images are shown for scrambled siRNA (CTL) and *NCOR1* knockdown (siNCOR1). Scale bars indicate 50 μm. **(F)** Quantification of NCOR1-RBPJk interactions per nucleus. n = 3, Unpaired *t*-test. $*P < 0.05$. **(G)** Reporter gene assay of HUVEC after siRNA-mediated knockdown of *NCOR1* (NCOR1) or scrambled siRNA as negative control (CTL) in cells transfected with GL4[luc2P_empty vector] (CTL) or pGL4[luc2P_RBP-Jk-RE] vector (RBPJk). 24h after transfection, RBPJk-dependent luciferase activity was measured by dual-luciferase reporter gene assay and luminescence measurement. n = 3, One-way ANOVA. $*P < 0.05$. **(H&I)** Spheroid outgrowth assay of HUVECs with and without siRNA-mediated knockdown as indicated. Scrambled siRNA served as negative control (CTL). Spheroids were treated with or without VEGF-A. Quantification of cumulative sprout length is shown. n = 3, One-way ANOVA. $*P < 0.05$.

corepressors to endothelial gene expression. We observed that *NCOR1* was the most highly expressed gene within this class and that knockdown of *NCOR1*, but not of the second and third most highly expressed repressors, *SMRT* and *REST*, promoted endothelial angiogenic function. Downregulation or knockout of *NCOR1* in endothelial cells increased branching capacity as well as outgrowth from spheroids or arteries kept in organ culture. Mechanistically, NCoR1 suppressed numerous angiogenic genes, among them VEGF receptors, genes of the Notch family as well Notch target genes. Depletion of RBPJk - a direct NCOR1 interactor - as well as NOTCH4, whose expression was induced in response to *NCOR1* knockdown, prevented the pro-angiogenic response associated with knockdown of *NCOR1*.

Eukaryotic cells living in a tissue context require a tight control of gene expression. An important function of epigenetics is the stabilization of the cellular gene expression state [47]. In particular through histone modifications, it is ascertained that cells maintain a phenotypic state and a certain amount of "activation energy" is therefore required to move the cell from the execution of one gene expression program to the next. Within this control mechanism, corepressors have an important function as they serve as docking platform for chromatin modifying enzymes and are also subject to regulation by post-translational modification, like phosphorylation, which result in their nuclear export and degradation [48].

In general, it is not completely clear how the individual corepressors mediate specific functions. As scaffolding proteins, most corepressors lack DNA binding sides and only interact with other proteins in a dynamic fashion. During gene repression, corepressors form a complex with HDACs and transcription factors. Upon stimulation, the corepressors are displaced, which also removes the HDAC from the vicinity of the gene, subsequently allowing recruitment of histone acetyltransferase, followed by gene activation [49]. Different signal transduction pathways converge on different corepressors. In this regard, comparisons between NCoR1 and SMRT have been performed [50]. SMRT is a downstream target of MEKK1, an important kinase of the mitogen-activated protein kinase (MAPK) pathway, which is activated by receptor tyrosine kinases like the epidermal growth factor receptor (EGFR) or the VEGF receptors. NCoR1, however, is refractory to MEKK1 phosphorylation [51]. This observation links SMRT to proliferative responses. NCoR1, in contrast, appears to contribute to inflammatory signaling: IL-1β stimulation of cells results in NCoR1 nuclear export, while SMRT is not affected [52]. Akt, selectively acts on the cytosolic retention of NCoR1, through phosphorylation of serine 401 in the Gal4 DNA-binding domain. As SMRT contains an alanine residue at this position, it is not targeted by Akt [53]. Collectively, corepressors exert distinct biological actions depending on the cell type, the expression level and the phosphorylation state [54].

Although NCoR1 is among the best-characterized nuclear corepressors, its function in the angiogenic program and in endothelial cells has not yet been studied. It was therefore unexpected to observe that loss of NCoR1 selectively promoted an angiogenic phenotype and did not result in basal inflammatory activation or uncontrolled proliferation. This suggests that the endothelial environment provide cues for angiogenesis rather than for the other gene programs. In fact, we observed that depending on the model, different angiogenic properties of the endothelial cell were affected. RNA-seq of cells in 2D monolayer culture demonstrated a de-repression of classic angiogenic genes, like VEGF receptors, after NCoR1 depletion. Despite this, KRN633, a pan-VEGF receptor inhibitor, abolished VEGF-driven angiogenesis, but not *NCOR1* depletion mediated angiogenesis. This suggests that VEGF receptor expression is more so a consequence than a cause of the *NCOR1* depletion-mediated angiogenic response. In fact, endothelial cells are not equally sensitive to VEGF, but exhibit cellular specification driven by other receptor-dependent pathways, like WNT, FOXO or Notch, resulting in variation in VEGF receptor expression [55]. Given the multitude of endothelial cues specifying for angiogenesis, it is difficult to infer relevant pathways. To solve this problem, we performed ATAC-seq. Using these data, information about occupation of transcription factor binding sites in the vicinity of genes can be gathered, and gene activation state can be inferred. Using the software TEPIC, ATAC-seq together with RNA-seq can be integrated to predict the transcription factors actively binding to a gene with high certainty [35]. Results of this analysis pointed towards a tip cell specification and the Notch pathway playing a significant role in the observed effects of NCoR1 depletion. The fact that RBPJk was not among the top hits, can be explained by its context specific function. RBPJk acts as part of an activator or repressive complex, hence binding affinity itself remains rather unchanged [56].

Interestingly, a link between RBPJk and NCoR1 has previously been suggested. In a quiescent cell state, RBPJk is the key transcription factor repressing Notch target genes, first shown in *Drosophila* [57]. Upon binding of Notch intracellular domain (NICD), the interacting corepressors are replaced with coactivators. However, the mechanistic details are controversial, because the NCoR1 corepressor complex was reported to interact with RBPJk through its binding partner SHARP [58], whereas another study suggested involvement of TBL1 and TBLR1 [59]. Our data gathered from proximity ligation assays suggest that the interaction between NCoR1 and RBPJk is fairly direct in endothelial cells.

NCoR1 depletion increased the expression of *NOTCH1*, *NOTCH2* and especially *NOTCH4* as well as Notch-specific target genes *HEY1* and *HEY2*. In endothelial cells, Notch signaling plays an important role in cell specification and contributes to tip and stalk cell selection during sprouting angiogenesis. It is therefore unsurprising that similar to NCoR1, Notch is important for embryonic development and often affected in cancer [60]. Notch can be activated by several stimuli among them DLL4, which is secreted from tip cells to maintain the phenotype of stalk cells [61]. In the present study, a significant upregulation of *DLL4* expression in NCoR1-depleted cells was observed, which was paralleled by an induction of Notch target genes. These gene expression data, however, do not fit to the functional observations of the present study, suggesting hypersprouting [62]. In fact, the opposite should have occurred: Notch activation should decrease sprouting whereas inhibition of Notch signaling (e.g. with DBZ) results in an inadequate high number of tip cells and so called hypersprouting [62]. This is exactly what was observed in the spheroid outgrowth assay after NCoR1

depletion, also suggesting a tip cell specification. As an explanation for this paradoxical response, we could demonstrate that not only *NOTCH1* but also *NOTCH4* is de-repressed by knockdown of *NCOR1*. Notch4 is primarily expressed in the vasculature, and was shown to act as endogenous inhibitor to Notch1, when expressed in *cis* [63]. This appears to be relevant in the present study, where knockdown of *NOTCH4*, but not *NOTCH1,* was able to block the hypersprouting phenotype induced by *NCOR1* knockdown.

Collectively, the present study demonstrates that NCoR1 contributes to the exact maintenance of endothelial gene expression programs. Decreasing *NCOR1* expression induces an angiogenic response in endothelial cells, albeit at the expense of a focused maintenance of gene expression programs, as shown by genome-wide chromatin opening. Therefore, long term depletion of NCoR1 does not appear to be an attractive strategy to maintain angiogenesis. In the context of acute scenarios like wound healing in diabetes, perturbation of NCoR1 might represent a therapeutic avenue to reinstate angiogenesis.

Source of funding

This study was supported by the Deutsche Forschungsgemeinschaft (DFG) projects: GRK2336 (AVE) Projektnummer 321115009, SFB1039 Projektnummer 204083920, SFB1531 Projektnummer 456687919, Cardio-Pulmonary Institute (CPI, EXC2026, Projektnummer 390649896B), the Goethe University, FrankfurtC) DZHK (Deutsches Zentrum für Herz-Kreislauf-Erkrankungen).

Declaration of Generative AI and AI-assisted technologies in the writing process

The authors did not use generative AI or AI-assisted technologies in the development of this manuscript.

CRediT authorship contribution statement

Tom Teichmann: Conceptualization, Data curation, Formal analysis, Investigation, Methodology, Validation, Visualization, Writing – original draft, Writing – review & editing. **Pedro Malacarne:** Investigation. **Simonida Zehr:** Formal analysis, Visualization. **Stefan Günther:** Investigation. **Beatrice Pflüger-Müller:** Investigation, Methodology. **Timothy Warwick:** Conceptualization, Data curation, Supervision, Visualization, Writing – original draft, Writing – review & editing. **Ralf P. Brandes:** Conceptualization, Funding acquisition, Project administration, Supervision, Validation, Visualization, Writing – original draft, Writing – review & editing.

Declaration of competing interest

The authors declare no conflict of interest.

Data availability

We have uploaded the RNA- and ATAC-Seq data into the public NCBI GEO database under the accession number GSE237654.

Acknowledgements

The authors are grateful for the excellent technical assistance of Katalin Pálfi and Judit Ponce.

Appendix A. Supplementary data

Supplementary data to this article can be found online at https://doi.org/10.1016/j.yjmcc.2024.02.003.

References

[1] O. Morrison, J. Thakur, Molecular complexes at Euchromatin, Heterochromatin and Centromeric Chromatin, IJMS 22 (2021) 6922, https://doi.org/10.3390/ijms22136922.
[2] A. Bannister, T. Kouzarides, Regulation of chromatin by histone modifications, Cell Res. 21 (2011) 381–395, https://doi.org/10.1038/cr.2011.22.
[3] G. Bowman, M. Poirier, Post-translational modifications of histones that influence nucleosome dynamics, Chem. Rev. 115 (2015) 2274–2295, https://doi.org/10.1021/cr500350x.
[4] V. Perissi, K. Jepsen, C. Glass, M. Rosenfeld, Deconstructing repression: evolving models of co-repressor action, Nat. Rev. Genet. 11 (2010) 109–123, https://doi.org/10.1038/nrg2736.
[5] N. Liang, T. Jakobsson, R. Fan, E. Treuter, The nuclear receptor-co-repressor complex in control of liver metabolism and disease, Front. Endocrinol. (Lausanne) 10 (2019) 411, https://doi.org/10.3389/fendo.2019.00411.
[6] O. Marescal, I. Cheeseman, Cellular mechanisms and regulation of quiescence, Dev. Cell 55 (2020) 259–271, https://doi.org/10.1016/j.devcel.2020.09.029.
[7] K. Jepsen, O. Hermanson, T. Onami, A. Gleiberman, V. Lunyak, R. McEvilly, et al., Combinatorial roles of the nuclear receptor corepressor in transcription and development, Cell 102 (2000) 753–763, https://doi.org/10.1016/S0092-8674(00)00064-7.
[8] K. Jepsen, D. Solum, T. Zhou, R. McEvilly, H.-J. Kim, C. Glass, et al., SMRT-mediated repression of an H3K27 demethylase in progression from neural stem cell to neuron, Nature 450 (2007) 415–419, https://doi.org/10.1038/nature06270.
[9] L. Müller, D. Hainberger, V. Stolz, W. Ellmeier, NCOR1-a new player on the field of T cell development, J. Leukoc. Biol. 104 (2018) 1061–1068, https://doi.org/10.1002/JLB.1RI0418-168R.
[10] H. Yamamoto, E. Williams, L. Mouchiroud, C. Cantó, W. Fan, M. Downes, et al., NCoR1 is a conserved physiological modulator of muscle mass and oxidative function, Cell 147 (2011) 827–839, https://doi.org/10.1016/j.cell.2011.10.017.
[11] C. Li, X.-N. Sun, B.-Y. Chen, M.-R. Zeng, L.-J. Du, T. Liu, et al., Nuclear receptor corepressor 1 represses cardiac hypertrophy, EMBO Mol. Med. 11 (2019), https://doi.org/10.15252/emmm.201809127.
[12] S. Oppi, S. Nusser-Stein, P. Blyszczuk, X. Wang, A. Jomard, V. Marzolla, et al., Macrophage NCOR1 protects from atherosclerosis by repressing a pro-atherogenic PPARγ signature, Eur. Heart J. 41 (2020) 995–1005, https://doi.org/10.1093/eurheartj/ehz667.
[13] Y. Lei, H. Haider, J. Shujia, E. Sim, Therapeutic angiogenesis. Devising new strategies based on past experiences, Basic Res. Cardiol. 99 (2004) 121–132, https://doi.org/10.1007/s00395-004-0447-x.
[14] B. Yu, S. Wang, Angio-LncRs: LncRNAs that regulate angiogenesis and vascular disease, Theranostics 8 (2018) 3654–3675, https://doi.org/10.7150/thno.26024.
[15] R. Lugano, M. Ramachandran, A. Dimberg, Tumor angiogenesis: causes, consequences, challenges and opportunities, Cell. Mol. Life Sci. 77 (2020) 1745–1770, https://doi.org/10.1007/s00018-019-03351-7.
[16] L. Lamalice, F. Le Boeuf, J. Huot, Endothelial cell migration during angiogenesis, Circ. Res. 100 (2007) 782–794, https://doi.org/10.1161/01.RES.0000259593.07661.1e.
[17] Z. Otrock, R. Mahfouz, J. Makarem, A. Shamseddine, Understanding the biology of angiogenesis: review of the most important molecular mechanisms, Blood Cells Mol. Dis. 39 (2007) 212–220, https://doi.org/10.1016/j.bcmd.2007.04.001.
[18] B. Yetkin-Arik, I. Vogels, N. Neyazi, V. van Duinen, R. Houtkooper, C. van Noorden, et al., Endothelial tip cells in vitro are less glycolytic and have a more flexible response to metabolic stress than non-tip cells, Sci. Rep. 9 (2019), https://doi.org/10.1038/s41598-019-46503-2.
[19] L.-K. Phng, F. Stanchi, H. Gerhardt, Filopodia are dispensable for endothelial tip cell guidance, Development 140 (2013) 4031–4040, https://doi.org/10.1242/dev.097352.
[20] R. Kopan, M. Ilagan, The canonical notch signaling pathway: unfolding the activation mechanism, Cell 137 (2009) 216–233, https://doi.org/10.1016/j.cell.2009.03.045.
[21] K. Tanigaki, T. Honjo, Two opposing roles of RBP-J in notch signaling, Curr. Top. Dev. Biol. 92 (2010) 231–252, https://doi.org/10.1016/S0070-2153(10)92007-3.
[22] D.-Y. Tian, X.-R. Jin, X. Zeng, Y. Wang, Notch signaling in endothelial cells: is it the therapeutic target for vascular Neointimal hyperplasia? IJMS 18 (2017) 1615, https://doi.org/10.3390/ijms18081615.
[23] Y. Wang, M. Nakayama, M. Pitulescu, T. Schmidt, M. Bochenek, A. Sakakibara, et al., Ephrin-B2 controls VEGF-induced angiogenesis and lymphangiogenesis, Nature 465 (2010) 483–486, https://doi.org/10.1038/nature09002.
[24] J. Schindelin, I. Arganda-Carreras, E. Frise, V. Kaynig, M. Longair, T. Pietzsch, et al., Fiji: an open-source platform for biological-image analysis, Nat. Methods 9 (2012) 676–682, https://doi.org/10.1038/nmeth.2019.
[25] A. Bolger, M. Lohse, B. Usadel, Trimmomatic: a flexible trimmer for Illumina sequence data, Bioinformatics 30 (2014) 2114–2120, https://doi.org/10.1093/bioinformatics/btu170.
[26] A. Dobin, C. Davis, F. Schlesinger, J. Drenkow, C. Zaleski, S. Jha, et al., STAR: ultrafast universal RNA-seq aligner, Bioinformatics 29 (2013) 15–21, https://doi.org/10.1093/bioinformatics/bts635.
[27] Y. Liao, G. Smyth, W. Shi, featureCounts: an efficient general purpose program for assigning sequence reads to genomic features, Bioinformatics 30 (2014) 923–930, https://doi.org/10.1093/bioinformatics/btt656.
[28] M. Love, W. Huber, S. Anders, Moderated estimation of fold change and dispersion for RNA-seq data with DESeq2, Genome Biol. 15 (2014), https://doi.org/10.1186/s13059-014-0550-8.

[29] UniProt: a worldwide hub of protein knowledge, Nucleic Acids Res. 47 (2019) D506–D515, https://doi.org/10.1093/nar/gky1049.
[30] J. Buenrostro, P. Giresi, L. Zaba, H. Chang, W. Greenleaf, Transposition of native chromatin for fast and sensitive epigenomic profiling of open chromatin, DNA-binding proteins and nucleosome position, Nat. Methods 10 (2013) 1213–1218, https://doi.org/10.1038/nmeth.2688.
[31] B. Langmead, S. Salzberg, Fast gapped-read alignment with bowtie 2, Nat. Methods 9 (2012) 357–359, https://doi.org/10.1038/nmeth.1923.
[32] P. Danecek, J. Bonfield, J. Liddle, J. Marshall, V. Ohan, M. Pollard, et al., Twelve years of SAMtools and BCFtools, GigaScience 10 (2021), https://doi.org/10.1093/gigascience/giab008.
[33] F. Ramírez, F. Dündar, S. Diehl, B. Grüning, T. Manke, deepTools: a flexible platform for exploring deep-sequencing data, Nucleic Acids Res. 42 (2014) W187–W191, https://doi.org/10.1093/nar/gku365.
[34] Y. Zhang, T. Liu, C. Meyer, J. Eeckhoute, D. Johnson, B. Bernstein, et al., Model-based analysis of ChIP-Seq (MACS), Genome Biol. 9 (2008) R137, https://doi.org/10.1186/gb-2008-9-9-r137.
[35] F. Schmidt, F. Kern, P. Ebert, N. Baumgarten, M. Schulz, TEPIC 2-an extended framework for transcription factor binding prediction and integrative epigenomic analysis, Bioinformatics 35 (2019) 1608–1609, https://doi.org/10.1093/bioinformatics/bty856.
[36] N. de Souza, The ENCODE project, Nat. Methods 9 (2012) 1046, https://doi.org/10.1038/nmeth.2238.
[37] R. Jones, J. Karkanias, M. Krasnow, A. Pisco, S. Quake, J. Salzman, et al., The Tabula Sapiens: A multiple-organ, single-cell transcriptomic atlas of humans, Science 376 (2022), https://doi.org/10.1126/science.abl4896.
[38] Single-cell transcriptomics of 20 mouse organs creates a tabula Muris, Nature 562 (2018) 367–372, https://doi.org/10.1038/s41586-018-0590-4.
[39] M. Martens, A. Ammar, A. Riutta, A. Waagmeester, D. Slenter, K. Hanspers, et al., WikiPathways: connecting communities, Nucleic Acids Res. 49 (2021) D613–D621, https://doi.org/10.1093/nar/gkaa1024.
[40] S.-Y. Park, J.-S. Kim, A short guide to histone deacetylases including recent progress on class II enzymes, Exp. Mol. Med. 52 (2020) 204–212, https://doi.org/10.1038/s12276-020-0382-4.
[41] F. Schmidt, N. Gasparoni, G. Gasparoni, K. Gianmoena, C. Cadenas, J. Polansky, et al., Combining transcription factor binding affinities with open-chromatin data for accurate gene expression prediction, Nucleic Acids Res. 45 (2017) 54–66, https://doi.org/10.1093/nar/gkw1061.
[42] J. Xie, L. Lin, X. Huang, R. Gan, L. Ding, B. Su, et al., The NOTCH1-HEY1 pathway regulates self-renewal and epithelial-mesenchymal transition of salivary adenoid cystic carcinoma cells, Int. J. Biol. Sci. 16 (2020) 598–610, https://doi.org/10.7150/ijbs.36407.
[43] Y. Yoshitomi, T. Ikeda, H. Saito-Takatsuji, H. Yonekura, Emerging role of AP-1 transcription factor JunB in angiogenesis and vascular development, IJMS 22 (2021) 2804, https://doi.org/10.3390/ijms22062804.
[44] W. Chen, P. Xia, H. Wang, J. Tu, X. Liang, X. Zhang, et al., The endothelial tip-stalk cell selection and shuffling during angiogenesis, J. Cell Commun. Signal. 13 (2019) 291–301, https://doi.org/10.1007/s12079-019-00511-z.
[45] M. Brzozowa-Zasada, The role of notch ligand, Delta-like ligand 4 (DLL4), in cancer angiogenesis—implications for therapy, Eur. Surg. 53 (2021) 274–280, https://doi.org/10.1007/s10353-021-00707-x.
[46] A. James, J. Szot, K. Iyer, J. Major, S. Pursglove, G. Chapman, et al., Notch4 reveals a novel mechanism regulating notch signal transduction, Biochim. Biophys. Acta (BBA) - Mol. Cell Res. 1843 (2014) 1272–1284, https://doi.org/10.1016/j.bbamcr.2014.03.015.
[47] W. Reik, Stability and flexibility of epigenetic gene regulation in mammalian development, Nature 447 (2007) 425–432, https://doi.org/10.1038/nature05918.
[48] L. Xu, C. Glass, M. Rosenfeld, Coactivator and corepressor complexes in nuclear receptor function, Curr. Opin. Genet. Dev. 9 (1999) 140–147, https://doi.org/10.1016/S0959-437X(99)80021-5.
[49] J. Torchia, C. Glass, M. Rosenfeld, Co-activators and co-repressors in the integration of transcriptional responses, Curr. Opin. Cell Biol. 10 (1998) 373–383, https://doi.org/10.1016/S0955-0674(98)80014-8.
[50] A. Mottis, L. Mouchiroud, J. Auwerx, Emerging roles of the corepressors NCoR1 and SMRT in homeostasis, Genes Dev. 27 (2013) 819–835, https://doi.org/10.1101/gad.214023.113.
[51] B. Jonas, M. Privalsky, SMRT and N-CoR corepressors are regulated by distinct kinase signaling pathways, J. Biol. Chem. 279 (2004) 54676–54686, https://doi.org/10.1074/jbc.M410128200.
[52] S. Baek, K. Ohgi, D. Rose, E. Koo, C. Glass, M. Rosenfeld, Exchange of N-CoR corepressor and Tip60 coactivator complexes links gene expression by NF-kappaB and beta-amyloid precursor protein, Cell 110 (2002) 55–67, https://doi.org/10.1016/s0092-8674(02)00809-7.
[53] O. Hermanson, K. Jepsen, M. Rosenfeld, N-CoR controls differentiation of neural stem cells into astrocytes, Nature 419 (2002) 934–939, https://doi.org/10.1038/nature01156.
[54] M. Privalsky, The role of corepressors in transcriptional regulation by nuclear hormone receptors, Annu. Rev. Physiol. 66 (2004) 315–360, https://doi.org/10.1146/annurev.physiol.66.032802.155556.
[55] M. Simons, E. Gordon, L. Claesson-Welsh, Mechanisms and regulation of endothelial VEGF receptor signalling, Nat. Rev. Mol. Cell Biol. 17 (2016) 611–625, https://doi.org/10.1038/nrm.2016.87.
[56] Z. Yuan, B. VanderWielen, B. Giaimo, L. Pan, C. Collins, A. Turkiewicz, et al., Structural and functional studies of the RBPJ-SHARP complex reveal a conserved corepressor binding site, Cell Rep. 26 (2019) 845–854.e6, https://doi.org/10.1016/j.celrep.2018.12.097.
[57] J. Johnson, R. Macdonald, Notch-independent functions of CSL, Curr. Top. Dev. Biol. 97 (2011) 55–74, https://doi.org/10.1016/B978-0-12-385975-4.00009-7.
[58] F. Oswald, P. Rodriguez, B. Giaimo, Z. Antonello, L. Mira, G. Mittler, et al., A phospho-dependent mechanism involving NCoR and KMT2D controls a permissive chromatin state at notch target genes, Nucleic Acids Res. 44 (2016) 4703–4720, https://doi.org/10.1093/nar/gkw105.
[59] V. Perissi, C. Scafoglio, J. Zhang, K. Ohgi, D. Rose, C. Glass, et al., TBL1 and TBLR1 phosphorylation on regulated gene promoters overcomes dual CtBP and NCoR/SMRT transcriptional repression checkpoints, Mol. Cell 29 (2008) 755–766, https://doi.org/10.1016/j.molcel.2008.01.020.
[60] B. D'Souza, L. Meloty-Kapella, G. Weinmaster, Canonical and non-canonical notch ligands, Curr. Top. Dev. Biol. 92 (2010) 73–129, https://doi.org/10.1016/S0070-2153(10)92003-6.
[61] N. Ferrara, Pathways mediating VEGF-independent tumor angiogenesis, Cytokine Growth Factor Rev. 21 (2010) 21–26, https://doi.org/10.1016/j.cytogfr.2009.11.003.
[62] R. Blanco, H. Gerhardt, VEGF and notch in tip and stalk cell selection, Cold Spring Harb. Perspect. Med. 3 (2013) a006569, https://doi.org/10.1101/cshperspect.a006569.
[63] A. James, J. Szot, K. Iyer, J. Major, S. Pursglove, G. Chapman, et al., Notch4 reveals a novel mechanism regulating notch signal transduction, Biochim. Biophys. Acta 2014 (1843) 1272–1284, https://doi.org/10.1016/j.bbamcr.2014.03.015.